ASTROBIOLOGY
Volume 6, Number 4, 2006
© Mary Ann Liebert, Inc.

Hypothesis Paper

Spiders: Water-Driven Erosive Structures in the Southern Hemisphere of Mars

OLGA PRIETO-BALLESTEROS, DAVID C. FERNÁNDEZ-REMOLAR, JOSÉ ANTONIO RODRÍGUEZ-MANFREDI, FRANCK SELSIS,* and SUSANNA C. MANRUBIA

ABSTRACT

Recent data from space missions reveal that there are ongoing climatic changes and erosive processes that continuously modify surface features of Mars. We have investigated the seasonal dynamics of a number of morphological features located at Inca City, a representative area at high southern latitude that has undergone seasonal processes. By integrating visual information from the Mars Orbiter Camera on board the Mars Global Surveyor and climatic cycles from a Mars' General Circulation Model, and considering the recently reported evidence for the presence of water-ice and aqueous precipitates on Mars, we propose that a number of the erosive features identified in Inca City, among them spiders, result from the seasonal melting of aqueous salty solutions. Key Words: Water—Erosive processes—Mars—Seasonal changes—Dark spots. Astrobiology 6, 651–667.

INTRODUCTION

DARK SPIDERS (Kieffer *et al*., 2000) are among the most intriguing morphological structures of the martian surface. A spider consists of a depressed region with branching radial troughs. It has been proposed that abrupt expulsions of gas are the main mechanism involved in their formation (Piqueux *et al*., 2003). Though those jets of CO_2 play a role in the local transport of dust and explain the fan-shaped deposits around the emission center, they do not seem to account for the carved, branched pattern that constitutes the most remarkable feature of spider morphology. The CO_2 jets hypothesis by Piqueux *et al*. (2003) requires the formation of spiders to be associated with the cryptic region, low albedo areas with temperatures around that of CO_2 sublimation during most of the year (Kieffer *et al*., 2000). Penetration of the sunlight to the base of the seasonal frost produces sublimation from the bottom, which breaks up the CO_2 layer and ejects the dust from the ground up. This process can occur because the low albedo of the ground absorbs more energy than brighter areas. Even pockets of dust into the seasonal polar cap could suffer this local heating (Kieffer *et al*., 2000). However, though this hypothesis explains the erosion by repeated outburst from year to year, the resulting branching geomorphology observed on the

Centro de Astrobiología, Instituto Nacional de Técnica Aeroespacial-Consejo Superior de Investigaciones Científicas, Ctra. Ajalvir km. 4, 28850 Torrejón de Ardoz, Madrid, Spain.
*Now at Ecole Normale Supérieure de Lyon, France.

ground does not correspond to a geyser-like process. The process can fracture the ice and move the gas with dust from the base of the structure, but how can gas possibly form the negative topography with radial drainage patterns? The observed crater morphology of spiders is more likely to be the result of an explosion initiated by superheated gas [similar to the Porkchop Geyser in Yellowstone Park (Fournier *et al*., 1991)].

A general survey of the region where spiders appear shows a number of related features apparently the results of the seasonal frosting and defrosting of ice, which suggests that a more general erosive mechanism is at work. On Earth, water melting in periglacial regions produces erosive landforms such as moulins or kettles whose characteristics are consistent with structures found on Mars (Malin and Edgett, 2001). In addition, water-rich glacial systems analogous to the terrestrial ones have been recognized (Kargel and Strom, 1992). Mars Odyssey (Titus *et al*., 2003) and Mars Express have detected the presence of surface water in the form of ice layers exposed at high southern latitude and as near surface and subsurface water-ice reservoirs from mid- to high latitudes (Boyton *et al*., 2002; Feldman *et al*., 2002; Mitrofanov *et al*., 2002; Bibring *et al*., 2004).

Although current conditions of the martian surface do not seem to be compatible with the presence of liquid water for long periods of time (Haberle *et al*., 2001), it has been suggested that water erosion created structures, such as gullies, at geologically recent ages (Malin and Edgett, 2001; Mellon and Phillips, 2001; Gaidos, 2001; Hartmann, 2001; Costard *et al*., 2002; Gilmore and Phillips, 2002; Mangold *et al*., 2004). However, other agents such as liquid CO_2 (Musselwhite *et al*., 2001) or mass wasting (Treiman, 2003) have been also considered with regard to the origin of these carved features. In fact, the concurrence of several factors [a favorable radiative balance, a reduced melting temperature by incorporation of salts (Marion, 2002; Marion *et al*., 2003), and the low thermal conductivity of the ice-rich regolith beds] can locally permit the presence of liquid water for short periods of several days on the martian surface.

Indirect proof of the existence of salts on the martian surface arose from infrared and X-ray fluorescence spectroscopy analyses obtained by the Viking landers (Clark and van Hart, 1981; Banin *et al*., 1992) and by Alpha Proton X-ray Spectrometer analysis carried out by the Pathfinder rover (Rieder *et al*., 1997). Unquestionable evidence for the presence of salts has been provided by the Mars Exploration rovers Opportunity and Spirit, and the OMEGA instrument observations from the Mars Express Orbiter (Christensen *et al*., 2004; Arvidson *et al*., 2005; Gendrin *et al*., 2005; Langevin *et al*., 2005; Morris *et al*., 2005). These observations suggest the local presence of ancient water masses that hosted sulfuric aqueous systems (Fairén *et al*., 2004) that contained Mg and Fe sulfates and chlorides (Kerr, 2004). This interpretation of ancient hydrologic conditions is compatible with the hypothesis of Knauth and Burt (2002) for the existence of brine aquifers characterized by melting temperatures well below that of pure water. Some authors have argued that brines would explain most of the recent aqueous features on Mars (Brass, 1980; Cabrol *et al*., 2001; Wynn-Williams *et al*., 2001). Laboratory experiments carried out with salty solutions prove that different mixtures of ionic complexes reduce the melting point for the NaCl-$CaCl_2$ salt system to less than 220K (*e.g.*, Borisenko, 1977). Moreover, the porous regolith and the hydrated salts act as excellent thermal insulators due to their low thermal conductivity (Prieto-Ballesteros and Kargel, 2005). Therefore, from late spring to early summer, when physical–chemical conditions increase the local temperature even above 258K, liquid water might be present for short periods of time (several days) on the martian surface. With these observations at hand, we propose that the water movement from underground reservoirs may explain the origin and growth of spider landforms.

The objective of this work is to constrain the origin of spiders. To do this we have followed the evolution of these features in the area of Inca City during two martian years using combined climatic and geomorphological data from several sensors. Both brightness temperature images from the Thermal Emission Imaging System (THEMIS) and the General Circulation Model (GCM) model have permitted identification of the effects of the local climate over the features. Mars Orbiter Camera (MOC) and Mars Orbiter Laser Altimeter (MOLA) sensors have provided data about the morphological changes throughout the various seasons. The possible roles of icy materials such as CO_2 and H_2O in the local area of Inca City have been traced by the temperature data. These data, when combined with image analysis over a two-martian-year period, indicate that spiders are features of erosive origin. A model to explain the formation of the spiders from stationary metastable salty liquid water is proposed.

GEOLOGY AND CLIMATE OF INCA CITY

During autumn and winter, for about 1 terrestrial year, sunlight is practically absent at latitudes greater than 60°S on Mars. However, these same areas can reach temperatures above 258K during the southern hemisphere summer (Table 1). We have selected the Inca City (a region between 55°–65°W and 78°–86°S) as a representative location where a wide range of surface temperatures occurs (Fig. 1). This region was emplaced late Noachian–early Hesperian (Kerr, 2004), and covers an area of about 50,000 km^2. Inca City is an elevated terrain at 2,000 m above the average martian level and is characterized by two sets of ridges perpendicular to each other that form squared areas reminiscent of ancient Inca

TABLE 1. SUMMARY OF THEMIS AND MOC IMAGES CORRESPONDING TO THE INCA CITY AREA

Thermal emission infrared spectrum				
Image	L_s *(°)*	T_{max} *(K)*	T_{min} *(K)*	*Season* (L_s)
I07417007	242.5	183.2	163.3	Spring 180–270°
I07754007	260.1	238.8	169.3	
I07779004	261.4	242.5	147.4	
I07829006	264.1	247.8	164.8	
I07879011	266.6	257.1	181.5	
I07904011	267.9	255.9	181.2	
I07954004	270.5	258.5	178.5	Summer 270–360°
I08266008	286.5	267.6	148	
I08291004	287.8	266.8	142.8	
I08915007	318.2	235.6	179.1	
I08940002	319.4	227.3	157.8	
I08990006	321.7	232.3	Buffered	
I00826006	330.1	224.4	Buffered	
I01550006	1.2	167	Buffered	Fall 0–90°

MOC			
Image	L_s *(°)*	*Agent*	*Season* (L_s)
E04-00193	162.6	CO_2	Winter 90–180°
E05-00821	175.5		
E06-00746	194.3		Spring 180–270°
R06-01343	208.3		
E07-00862	214		
E07-01476	218		
R07-01395	224.7		
R07-01997	230.2		
E08-01284	239		
R08-01665	243.9		
R08-01705	244.1		
R08-02518	250		
E08-01763	253		
E09-00679	249	CO_2–H_2O	
R09-01916	262		
E10-00944	267	H_2O	
R09-04077	269.9		
E11-01855	288		Summer 270–360°
E13-00006	319		
M13-01779	324		
M14-02193	344		
M16-00825	7.6		Fall 0–90°

In the second column we show the time (L_s) at which the image was taken. For THEMIS images (source http://www.themis-data.asu.edu), the maximum and minimum temperature (T) values in the areas surveyed are shown. We assume that direct measures of temperatures below 145K are erroneous and are in fact buffered by the equilibrium temperature of CO_2 sublimation. For MOC images (source http://www.msss.com), we indicate the agent involved in the spider-forming cycle, as deduced from the measured temperatures. The last column indicates in both cases the corresponding season of the martian year.

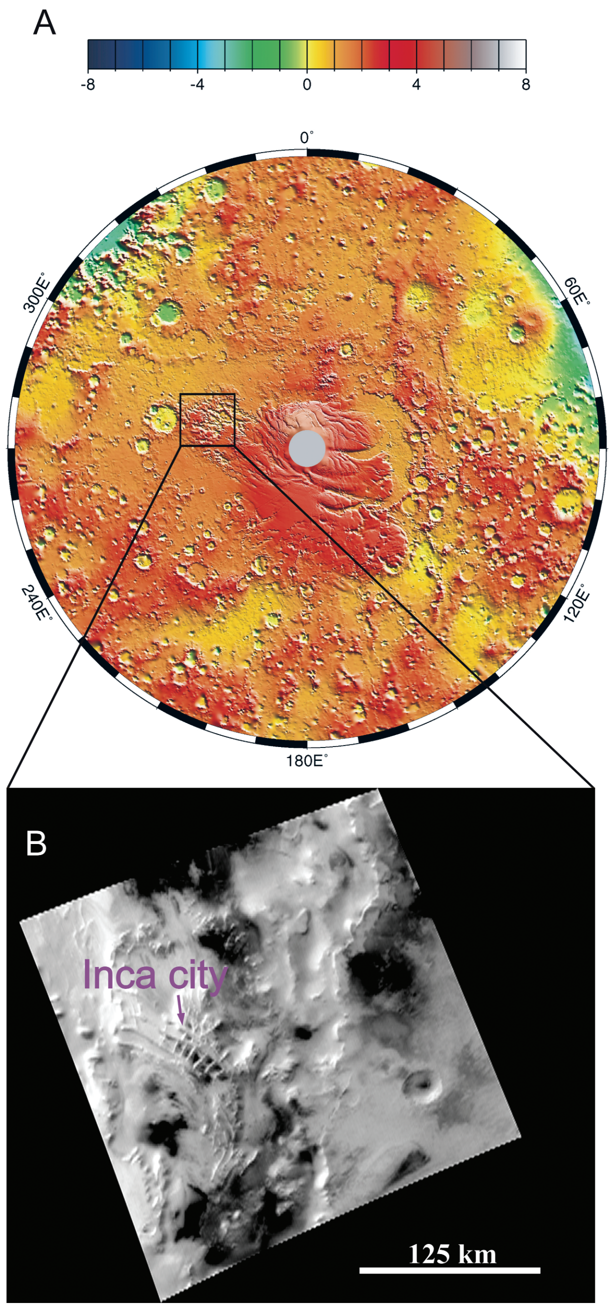

FIG. 1. (**A**) Location of Inca City in the southern martian hemisphere (color scale in kilometers). The image is artificially illuminated from the upper right and has been generated through elevation data from the MOLA device. (**B**) Major landforms in Inca City as seen in MOC image M0804693, at $L_s = 227.7°$, which shows the characteristic perpendicular ridges of glacial origin. The ridges delimit dark terrains with spiders, erosive channel-like structures, and depositional landforms. The arrow precisely points at Inca City in the general context.

constructs. Prominent slopes around this elevated region link it to the surrounding lower lands. Strata that correspond to the polar-layered deposits formation can be observed in MOC images along slopes in the northern Inca City region (Fig. 2). Two hypotheses have been proposed to explain the origin of the main geomorphologic features (*e.g.*, the ridges) of Inca City: (1) basal melting beneath the ice sheet and (2) discharge of clastic volatile material (Tanaka and Kolb, 2001).

The average climatic conditions at Inca City during the martian year have been obtained from a GCM of Mars (Lewis *et al.*, 1999). The total energy flux that reaches the surface has been calculated through a radiative transfer model that takes into account the optical depth measured by the Mars Global Surveyor (MGS) (Córdoba-Jabonero *et al.*, 2003). At the beginning of autumn in the southern hemisphere ($L_s = 0°$), the amount of sunlight that reaches the area is almost null. This produces a sharp decrease in the temperature, and CO_2 ice starts to accumulate. There are several effects related to the accumulation, presence, and eventual sublimation of CO_2 ice (Malin *et al.*, 2001; Byrne and Ingersoll, 2003). First, because of the release of energy that accompanies the phase change from vapor to solid, the surface is kept at equilibrium temperature for both the solid and gas phases. This temperature might oscillate, depending on the atmospheric pressure, between 145.9K (at 3 mbar) and 150.5K (at 10 mbar). At the same time, the ice isolates the surface below. Since CO_2 ice is fairly transparent in the visible range, a noticeable amount of energy reaches the interface between the seasonal ice and the terrain below. The ice is opaque in the thermal infrared, such that a solid-state greenhouse effect must be taking place at those sites. Experimental and theoretical investigations of this greenhouse effect conclude that increases in temperature of more than 50K could occur just a few centimeters below the exposed surface (Kaufmann *et al.*, 2002). The accumulation of CO_2 continues until about $L_s = 180°$, when spring begins and solar energy is again available. There is a delay of about 30° L_s between the time at which the Sun starts to illuminate the region and the moment at which the surface temperature increases, since for this period most of the energy is invested in ice sublimation. The ice cycle influences the local climatic conditions and slowly modifies the characteristics of these regions (see Fig. 3).

The GCM yields information on several climatic parameters at intervals of 30° L_s (seasonal longitude) with a precision of 5° latitude and longitude. However, the higher-precision data yielded by THEMIS show that the surface tem-

FIG. 2. Late winter MOC E0500821 image (L_s = 175.47°) showing a layered polar terrain located in northern Inca City. Dark spots are observed for the first time. White arrows (ds) indicate radial ejections from dark spots with a preferred orientation.

perature of the Inca City area displays strong variations. The brightness temperature is computed from the calibrated spectral radiance for band 3 of THEMIS, assuming a surface emissivity of 1.0 and an atmospheric opacity of 0.0. These assumptions allow us to infer a lower limit on the surface temperature, which would in fact be slightly higher than the observed brightness temperature. Band 3 was selected because it is the most transparent to dust and water ice, and the surface emissivity of most rock-forming minerals is near unity (Smith *et al.*, 2003). In particular, the confined depressions of Inca City show temperatures much higher (up to 60K) than surrounding regions at the same or even lower latitudes. Some images processed for late spring and early summer in the Inca City area present surface temperatures above 258K in slopes facing the Sun (northwest). As an example, image I07904011 (Fig. 4) shows a maximum temperature of 259K (L_s = 267.93°) for high areas protected against wind action, while a minimum of 202K is measured nearby. The average temperature of this image is 218.7K, in better agreement with the temperature predicted by the GCM. We ascribe the difference in temperature to a combination of different factors, among others (1) soil or rock composition and texture, which determine the thermal conductivity of the surface materials, and (2) topography and relief orientation, since they fix

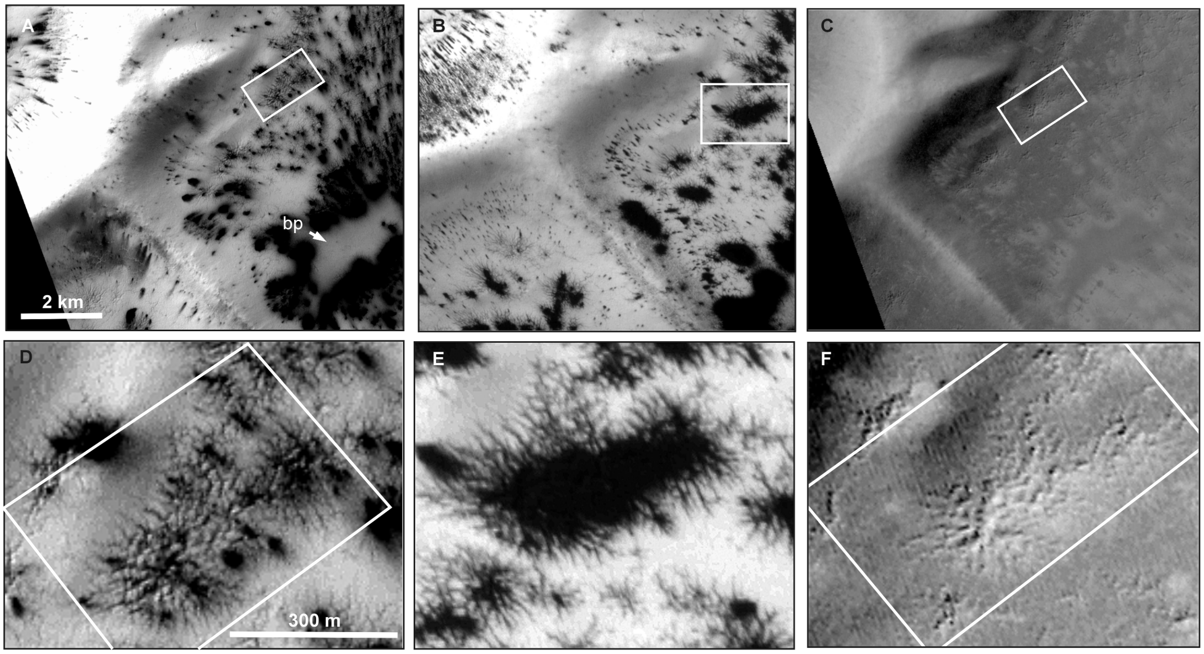

FIG. 3. MOC images showing small-scale features of the landscape (<1 km) occurring during the spring and summer of the martian southern hemisphere. (**A–C**) General views of the evolving landforms in two adjoining squared depressions at three different stages, from mid-spring to early summer. (**D–F**) Same morphological features at greater detail. (A) Image M0804693. Distribution of dark material in the square basins during mid-spring (L_s = 227.7°), apparently showing a transport of material from the outer ridges towards the center. The arrow indicates a bright patch of icy material (bp). (D) Erosive landforms with dendrites, where dark spots are preferentially localized. (B and E) In E0902750 (L_s = 263.13°), most of the dark material is concentrated at the bottom of the basin, mostly covering the erosive, spider-like features. The icy patch at the bottom has shrunk. (C and F) In summer, the dark material disappears, and, in the central area, the erosive features early described can be seen (MOC image E1100066, L_s = 282.4°).

the rate of insolation. Areas shielded against the south polar atmosphere might show temperatures much higher than the surrounding terrains. Taking into account the surface temperature measured by THEMIS from late spring to early summer in Inca City, and the plausible existence of salty aquifers associated with the South Pole permafrost, we propose that all of the erosive structures identified in Inca City (in particular spiders) result from seasonal defrosting of permafrost salty aquifers.

To register different data, MOC images have been corrected geometrically to the same projection. The analysis of narrow-angle MOC images reveals the existence of different structures that plausibly result from the yearly climatic oscillations. Most morphologies associated with spiders consist of polygonal terrains (Fig. 5), which occupy the inner depressions confined inside the perpendicular ridges of Inca City. Gullies (Fig. 6) and radial-displayed channels associated with aprons are also located on the slope of the confining ridges. Similar structures are observed in periglacial regions on Earth, where they are water-driven landforms that actively form during warm seasons. Polygonal fractured terrains grow cyclically by cryohydrostatic stress under the water active layer located above the permafrost that, as many authors have observed since the 1960s (*e.g.*, Alton Wade and Negus De Wys, 1968), is defrosted each year. On Mars, gullies and radial channeled aprons are formed yearly by either underground or surface defrosting water (Hartmann *et al.*, 2003). In other regions of Mars, the slope channeled structures have been proposed to result from frosting and defrosting cycles of aqueous solutions stored in soils and permafrost (Cabrol *et al.*, 2001; Haberle *et al.*, 2001; Wynn-Williams *et al.*, 2001; Costard *et al.*, 2002; Bennett and Glasser, 2003; Heldmann and Mellon, 2004).

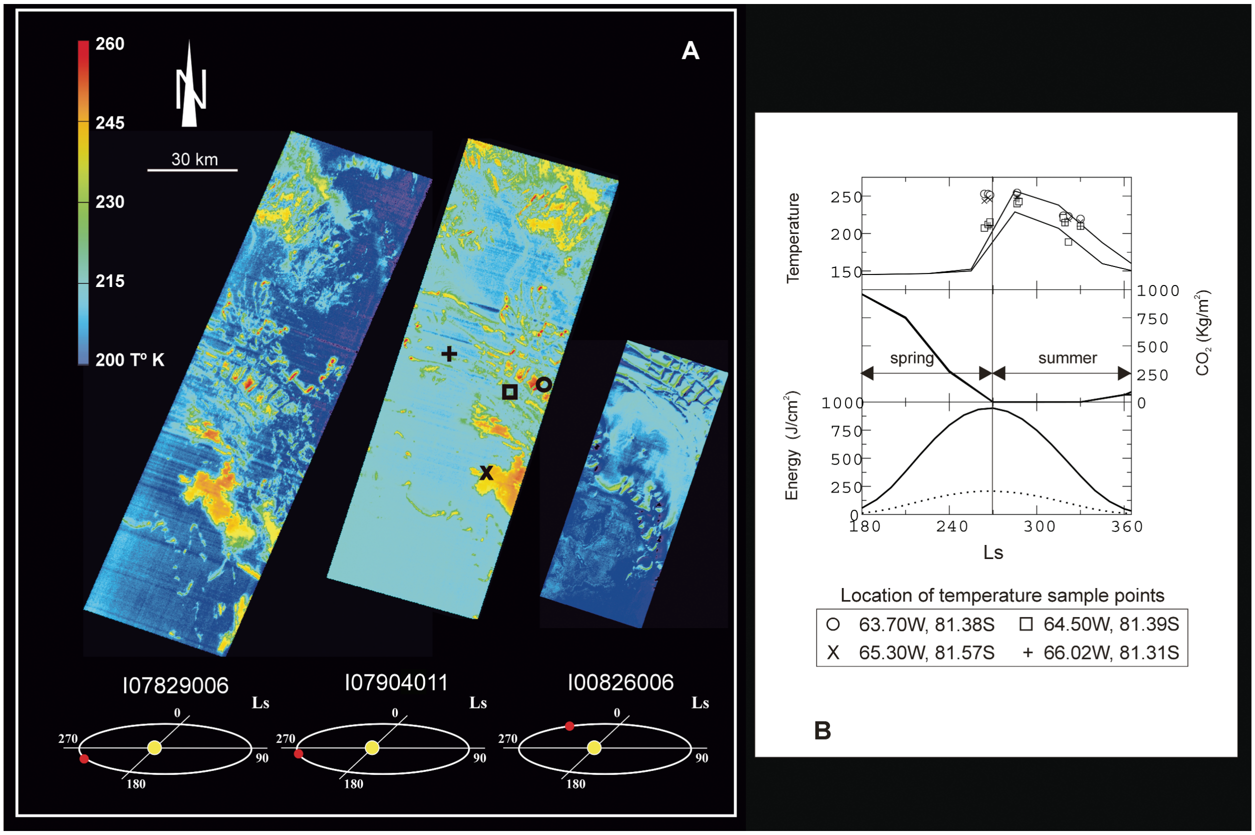

FIG. 4. Estimation of surface temperature acquired by THEMIS and obtained through the GCM model. (**A**) Changes in surface temperature in Inca City area at L_s = 267.9 sols obtained by THEMIS. Brightness temperature has been calculated from data in the third band for images I07829006 (L_s = 264.04°), I07904011 (L_s = 267.9°), and I00826006 (L_s = 321.74°). (**B**) Seasonal variation in temperature and CO_2 coverage (as predicted by the GCM) and in incident energy integrated in the ultraviolet and visible ranges at the latitude of the Inca City region. Direct measurements of brightness temperature carried out by THEMIS are shown as symbols in the same plot (see Table 1). Each point corresponds to one image pixel, and represents a square of 100 m on a side.

SEASONAL CYCLE OF SPIDER FORMATION AND ASSOCIATED LANDFORMS

All narrow- and wide-angle MOC images from AB to R09 phases of MGS corresponding to Inca City have been analyzed. They span different seasons and have revealed that the Inca City area has, indeed, a changing landscape and that the geomorphological processes involved seem to be driven by CO_2 and H_2O sublimation–melting cycles. As THEMIS data imply, such cycles are mostly regulated by thermal changes during the year, which allow CO_2 and H_2O phase changes. Solid CO_2 sublimation (beginning at 145K) and the presence of brines (possible already at 255K) take place at very different temperatures: by the time liquid water may be present, there is no trace of CO_2 in the region. Active spider-forming events start in late winter, when temperatures are well below that of CO_2 sublimation. By early fall, with temperatures lower than 160K, the cycle ends (Table 1). From the end of spring until midsummer, the temperature rises locally above 255K in several locations and for an extended period (between 30° and 60° L_s).

In the following sections, we describe in detail the seasonal changes the region undergoes and present a model aimed at explaining the formation of different erosive features, with an emphasis on spiders. To this end, we use MOC images and combine the visual information with the seasonal cycles just described. Representative images with the corresponding temperatures as measured with THEMIS are summarized in Table 1.

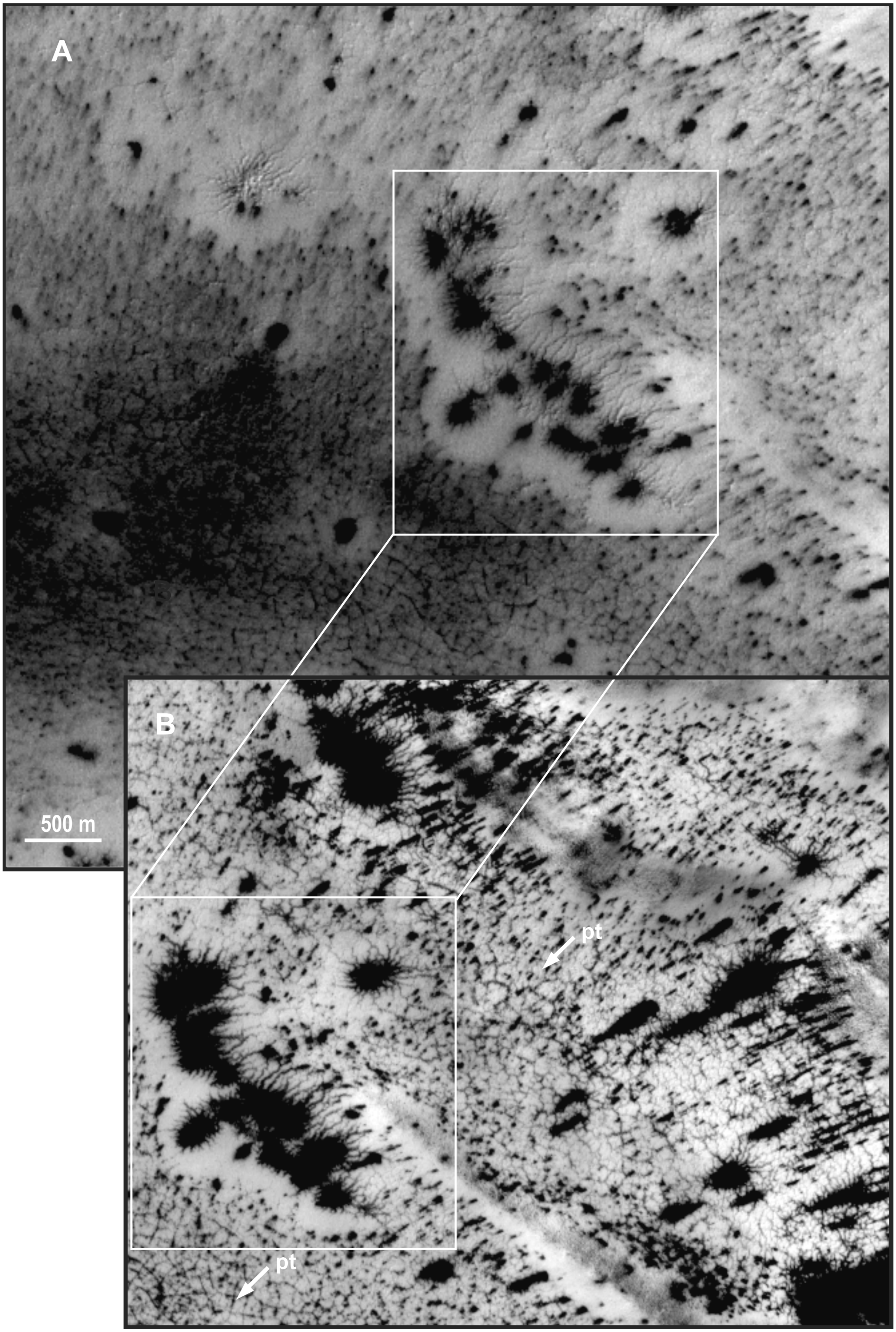
A
500 m
B
pt
pt

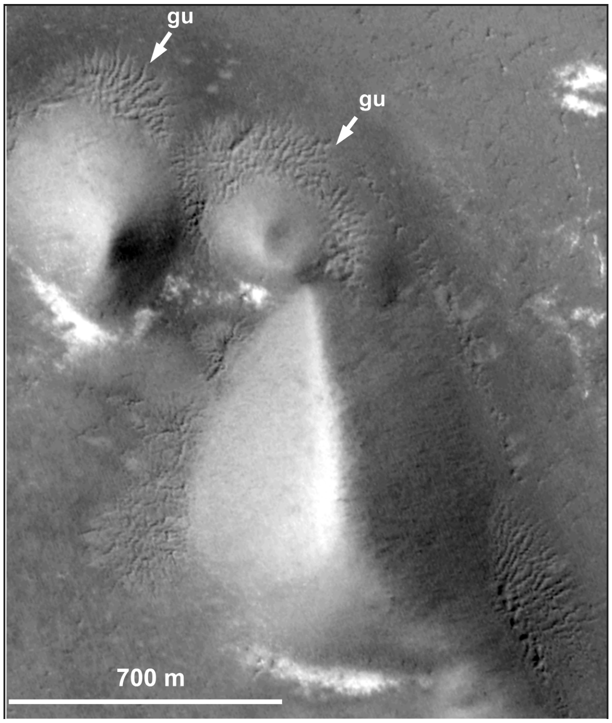

FIG. 6. MOC E1100066 image showing fan-patterned gullies at the base of some conic-shaped hills. White arrows indicate fan-shaped gullies (gu).

Pre-spider stage (late winter to early and middle spring)

In autumn and winter, CO_2 has accumulated and ice covers all of the region. Toward the end of winter, temperatures start to increase (see Fig. 4), and the CO_2 blanket decreases in both thickness and extension. The first MOC winter image analyzed (E0401193, L_s = 162.60°, Table 1) shows poorly contrasted low albedo terrains, except for the ridge highs, because of a low angle Sun illumination. Toward the end of winter (E0500821, L_s = 175.47°, see Fig. 2), new features (among them dark spots with fine material dispersed around them) appear on the deposits. Some layers show dark spots lined up along stratification levels. Dark spots have single or multiple radial ejections with a preferred orientation.

Since the surface temperature, though low, exceeds 140–150K, the appearance of dark spots has to be ascribed to CO_2 sublimation (Piqueux *et al.*, 2003). Although the mechanism of emission is not completely understood, Piqueux *et al.* (2003) suggested that basal sublimation of CO_2 ice results in geyser-like emissions of both gas and dust. An alternative possibility would be that such jets result from the dissociation of CO_2 clathrates (Kargel and Lunine, 1998). Such a mechanism would be responsible for the development of a primary generation of dark spots related to spiders. In fact, the location of dark spots occurring in early to mid-spring is only partly associated with the center of the spider or with its branches (Fig. 3). Some dark circular structures located either on the bottom of the squared depressions, or on the flat terrains northward of Inca City, occupy preexistent hollows that become spiders during late spring (Fig. 3). The distribution of dust around the dark spots is compatible with venting of CO_2 gas through weaknesses in the CO_2 ice crust covering. Later, these fine materials are redistributed all over the region through the action of wind and gravity.

A maximum temperature of 183K at L_s = 194.27° has been measured during early spring. This indicates that CO_2 sublimation to the atmosphere is active. At L_s = 214°, dark spots become ubiquitous, and some circular and elongated spots present tenuous radial projections emerging from their centers or from their major axes. Although some of the tailed and elongated spots may be due to wind action, most of them follow the maximal gradient of the terrain, which suggests that gravitational processes shape the spot morphology (Gánti *et al.*, 2003). Some dark spots have occasional bright haloes and are closely related to the cracks with radial geometry. Some squared depressions have extensive mantles of fine black materials covering its bottom, on top of which bright patches detach (Fig. 3A).

As spring advances, the density of dark spots on every kind of terrain, permafrost or layered units, notably increases. Tailed and close-to-cir-

FIG. 5. Seasonal changes that provide some insights in spider evolution. (**A**) Image E0701476, L_s = 218.44°. The dark material concentrates at the center of the spiders and at some of the dendritic ends. The dark spots have a preferential orientation probably because of wind action. (**B**) Same location as (A), image E1000944, L_s = 267.67°. The dark material occupies preferentially the center of the spider depression, implying that the transport of material is due to gravity. White arrows indicate polygonal terrains (pt).

cular dark spot distributions are essentially the same as in early spring images, populating the slopes and the bottom of the depressions, respectively. Dark spots tend to appear close to the boundary between ridges and flat bottoms, though smaller spots may be located along the ridges. As seen in Fig. 3, there are some differences in size and shape between the dark spots that appear at those two locations. The dark spots located at the flat bottoms and piedmont have circular morphologies. They are usually larger than 300 m in diameter and are typically surrounded by dark-gray haloes. These haloes, which contrast with the brighter areas surrounding them, may be interpreted as depression shadows due to either the accumulation of dark soil materials located close to the surface or the accumulation of dispersed material from the CO_2 eruption (Piqueux *et al.*, 2003). South to Inca City, other groups of dark spots on flat terrain range from elongated to circular and display dark haloes like those in the squared depressions (Fig. 3A). In these southern regions, the association between ice cracks and dark units is shifted; the materials do not lie exactly over the crack.

Spider-forming stage (late spring to early summer)

At $L_s = 264°$, the surface temperature increased in the surveyed areas above 247K, which implies that CO_2 has to be rejected as an agent involved in the processes observed because it sublimates at 150K at the mean atmospheric pressure of Mars of 7 mbar. During this stage, the main morphological feature is the relocation of the dark materials into the depressions occupied by the spiders. Considering that the dark deposits are consistently associated with spider structures, we propose that the main agent involved in sediment transport and in the growth of spiders by erosion is liquid water.

Given that the temperature required to melt salty permafrost ices can be reached through the combined heating effect produced by the low albedo of dark materials and the local topography (see Fig. 4 and Table 1), the downhill movement of aqueous solutions would have two effects: relocation and concentration of the disseminated dark materials. In this scenario, brines produced in the defrosting front migrate into the hollows through the radially converging channels, which grow yearly by erosion. At this stage, spiders are filled by low albedo material, here interpreted as melted water carrying fine dark deposits. The high albedo materials rimming different structures are tentatively identified as water ice with lower salt content.

THEMIS data show temperatures above 258K during late spring. Spiders are clearly visible, and the cracks converging to their centers are filled with dark material. Inside the depressions, dark material is transported back to the center of the basins as well (Figs. 7 and 8). Coalescence of dark spiders and overlapping of their deposits is frequently observed near the piedmonts. Polygonal terrains that occur to the south of the depressions are prominent and show irregular channelized patterns with a characteristic winding morphology (Fig. 5).

The observed erosive structures with preferential orientation along ridges (Fig. 7C) are consistent with the flowing of liquid-saturated mud.

Spider exhumation stage (mid-summer)

The dark material, which is visible in spring because of its low albedo compared with that of icy materials, is not visible in the summer. The exposure of the ice-free ground highlights the erosive character of the spider-like structure. Early summer MOC images, which show an ice-free terrain, reveal where the structures originated in the spring (Fig. 3F). Some of the exhumed spiders are surrounded by materials with a slightly higher albedo (as seen in MOC images), which we conjecture to be precipitated salts from the transient brines (Fig. 3C and F). Our hypothesis—that a fluid transporting fine dark materials drives the erosive process—is further supported by the observation that the radial erosive landforms coincide with the dark spiders in springtime.

The surface temperature rapidly decreases from mid-summer to early fall. Spiders and other associated landforms gradually become covered by a CO_2 ice blanket. Already in late summer, some THEMIS images yield minimal temperatures that approach the CO_2 condensation point (Fig. 4 and Table 1).

Dormant stage (late summer to winter)

THEMIS data show temperatures decreasing below the freezing point of brines and then to the condensation point of CO_2 (Table 1). Tempera-

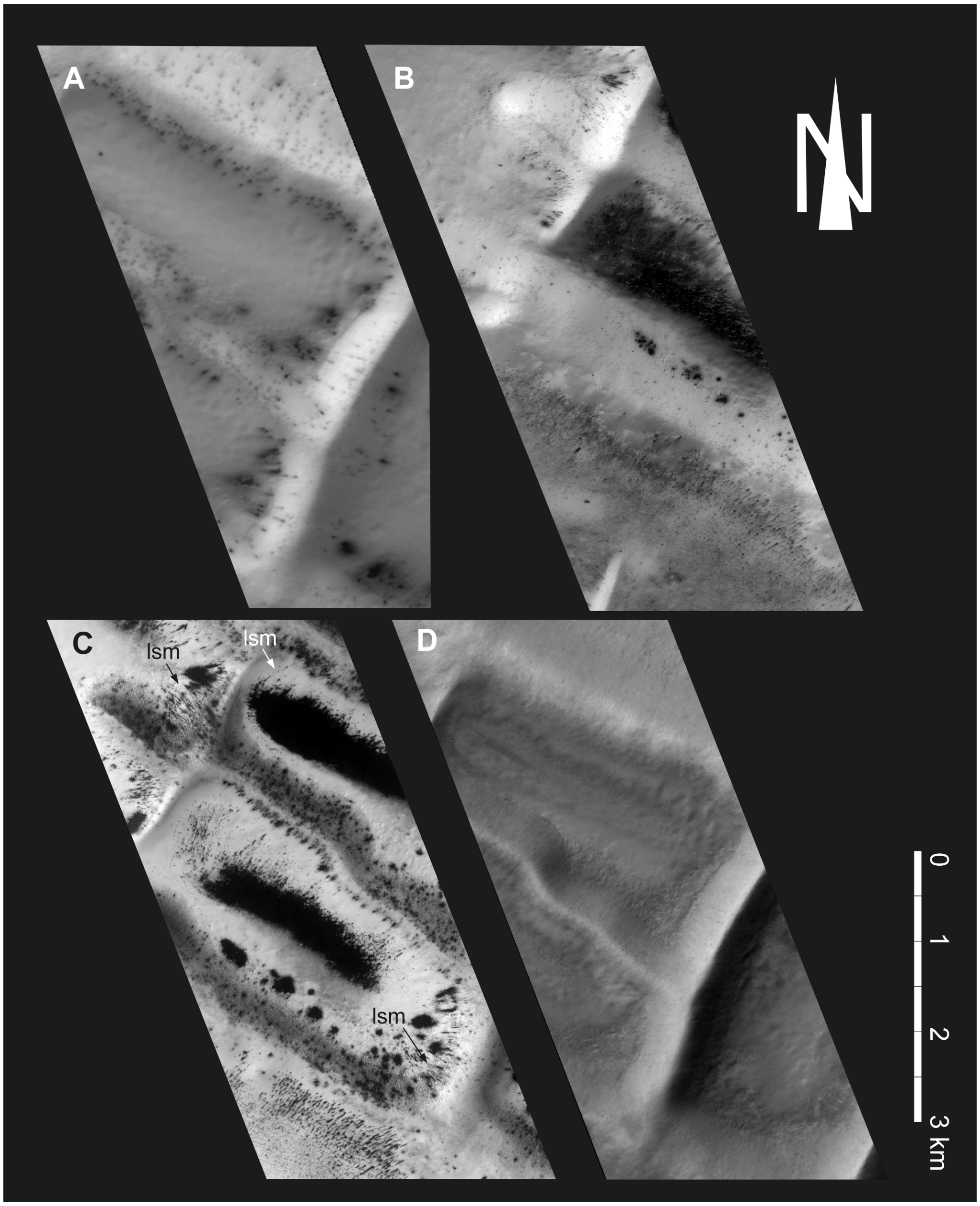

FIG. 7. Seasonal changes in the distribution of the inner dark deposits that transport from dispersed centers to confined basins: (A) E0600746 (L_s = 194.27°); (B) E0701476 (L_s = 218.44°); (C) E1000944 (L_s = 267°) [arrows indicate putative liquid-saturated material (lsm)]; (D) E1101376 (L_s = 286.18°).

ture data are not available in autumn, since the surface temperature falls below THEMIS sensitivity. The surface structures are covered by ice and kept inactive until the next year.

DISCUSSION

The period during which liquid water is present in Inca City can be roughly estimated as the time interval bound by the L_s of the first images showing dark material concentration and the L_s when dark spots disappear. At L_s = 263° (MOC image E09-02750) early hints of melted water are observed. Residual water bodies and exhumed spiders are recognized at L_s = 282° (MOC image E1100066, see Fig. 3C and F). Hence, the number of martian sols in which liquid water on the Inca City surface exists should be around 19. This time length agrees with independent theoretical esti-

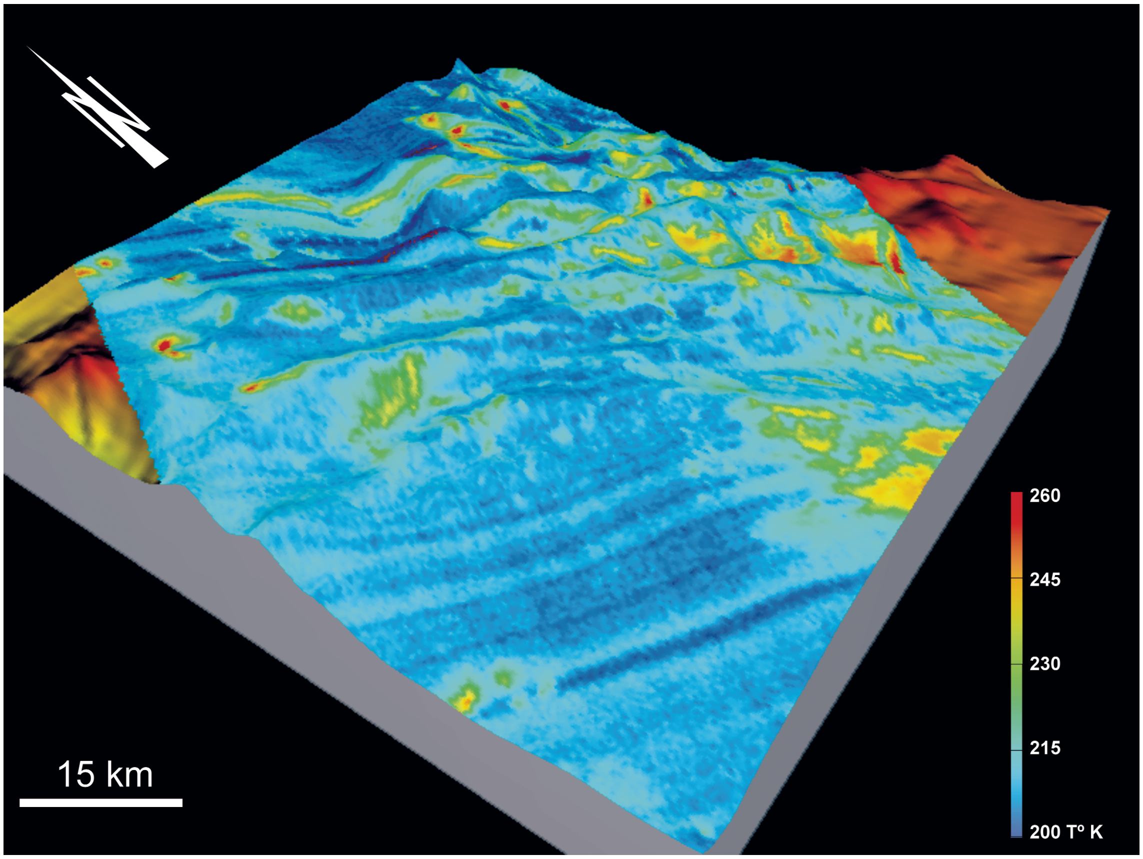

FIG. 8. Three-dimensional diagram that relates surface temperature and topography composed from MOLA and the 3 band of the I07904011 THEMIS image. The line-patterned structures seen in the front of the image are image artifacts.

mations carried out for Mars (Haberle *et al*., 2001; Kuznetz and Gan, 2002).

Periglacial and glacial regions of Earth show hollows topographically similar to martian spiders (Fig. 9). Such structures, known as kettles, consist of an enclosed hollow formed by the meltout of buried ice (Bennett and Glasser, 2003) and radial and branching channels that converge to the landform center. Seasonal evolution of the terrestrial kettles indeed shares some features with that of spiders. In the cold season, kettles are filled by ice, which increases their volume while the surface temperature is kept close to the melting point of the ice. During this process, the radial branches and the central hollow expand outward from the structure and produce a domed morphology. During the warm season, kettles act as collectors of meltwater that runs out through the radial channels from frozen soils and permafrost (Fig. 9). Some other landforms observed in Inca City are consistent with the existence of periglacial processes that have been hypothesized to act on the surface of southern Mars (Tanaka and Kolb, 2001).

A comparison at larger spatial scales between the landforms associated with kettles and the ridges enclosing spiders suggests that the geomorphologic features of Inca City can be modeled by ice retreat (Tanaka and Kolb, 2001). The exposure of underlying materials during ice degradation would make available huge volumes of frozen water that could melt if appropriate thermal and chemical conditions held, as seems to be the case. The existence of frozen water in the Inca City region supports the location of ice water reservoirs at high latitude during interglacial periods (Head *et al*., 2003). Current environmental conditions, together with the potential for seasonal water availability, define a microclimate comparable to that of cryophilic organisms in the coldest areas of Earth (Gánti *et al*., 2003; Jakosky *et al*., 2003).

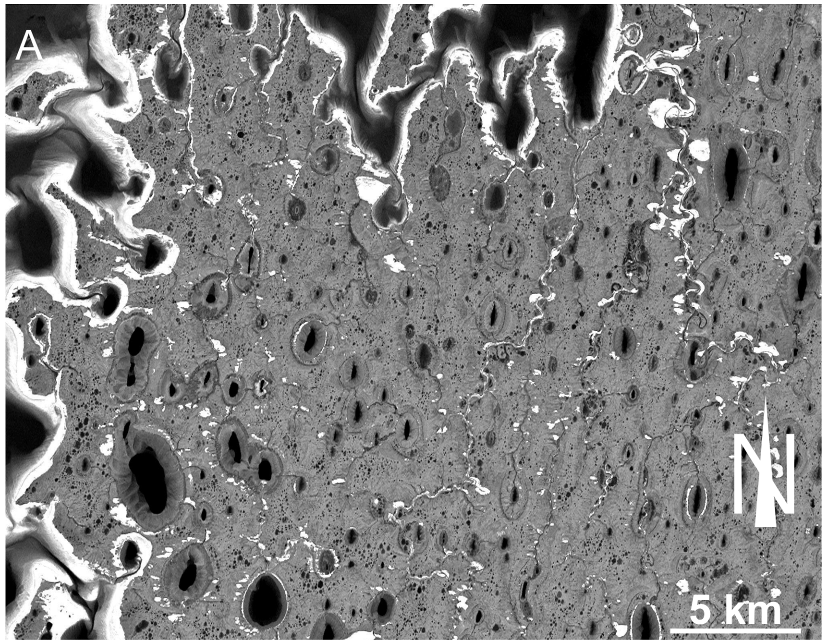

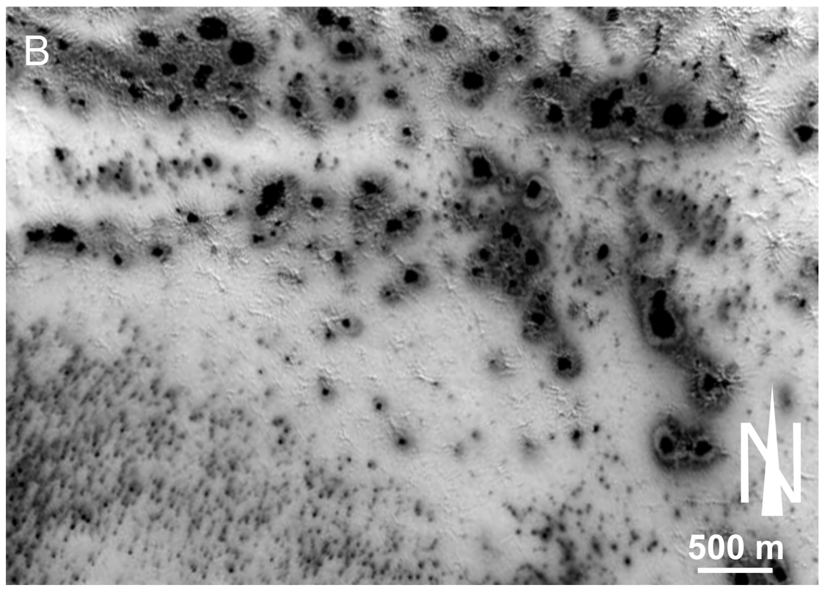

FIG. 9. Comparison between terrestrial kettles (ASTER image AST_07_003080320000411180000000) and spider-related dark spots (MOC image R08-01705). (**A**) Glaciofluvial ice-marginal landforms in Alaska (123°53′42″E and 73°29′06″N) consist of lakes and pools originated by the meltout of buried ice, conferring on the landscape a karstic pattern. Besides underground aquifers, surface water is transported to the kettle depressions, and radial channels converging to the depression center are formed. (**B**) Dark spotted structures on Mars show a similar pattern with radial channels. Spiders underlie these structures.

SUMMARY

We propose that spider evolution results from the seasonal changes in temperature that produce CO_2 phase changes and melt briny ices. During winter (Fig. 10A), the condensation of CO_2 ice buffers the surface temperature within the range of 145.9–150.5K, depending on the atmospheric pressure. In early spring (Fig. 10B), the surface temperature increases above 200K and sublimates the seasonal CO_2 ice layer, which is heated from below as a result of the solid greenhouse effect that occurs inside the CO_2 ice layer. Moreover, the rapid gas emissions during the spring (as explained by Piqueux *et al.*, 2003) eject material from the ground and disperse it on the surface. As a consequence of continuous heating, the seasonal CO_2 ice layer sublimates. In late spring (Fig. 10C), the ground temperature rapidly increases, which melts the water-ice layer and the salty permafrost. Any dispersed material is then suspended in the water and transported to lower topographic areas, which accentuates the drainage features characteristic of the spider morphology. Since liquid water is unstable under the current Mars atmospheric conditions, spiders

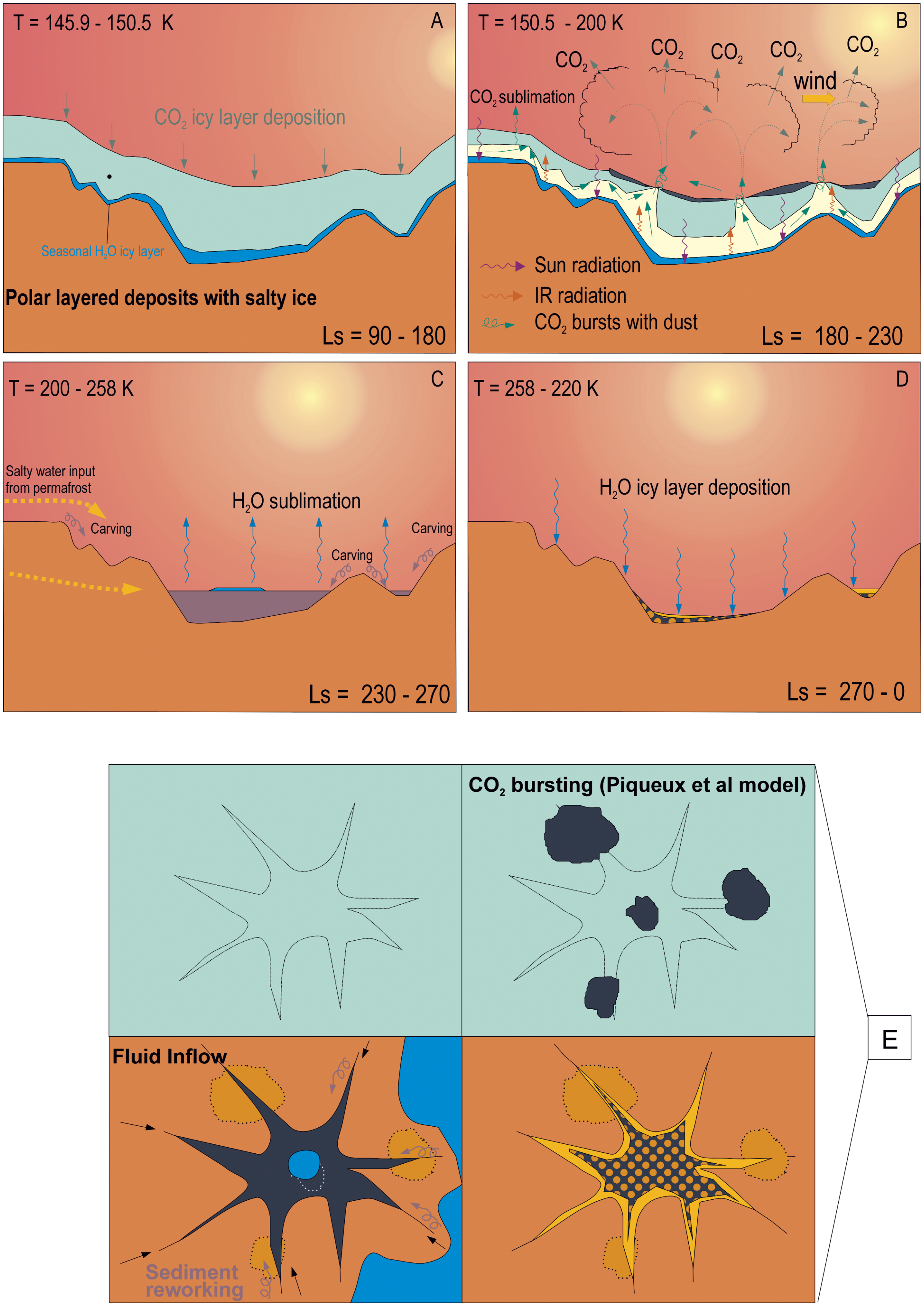

FIG. 10. Sketch describing spider evolution as a result of seasonal changes in temperature. (**A** and **B**) Pre-spider stages in winter (**A**) and early spring (**B**). IR, infrared. (**C**) Spider-forming stage in late spring. (**D**) Exhumation stage in summer. (**E**) Polar view of stages (A–D).

grow at a slower rate when compared with analogous terrestrial structures. High albedo patches observed in the MOC images are interpreted as salt precipitates from briny solutions associated with the spiders. Spectral data from instruments with spatial resolution higher than that of THEMIS will be needed to determine the composition of such deposits. Since any loose material will be re-ejected during the next spring season, it is removed from the region seasonally and does not fill up the basins. Finally, in mid-summer (Fig. 10D), the surface temperature decreases below the water condensation point, which favors the formation of a thin water-ice layer.

ACKNOWLEDGMENTS

The authors acknowledge fruitful discussions with E. Szathmáry, Sz. Berczi, A. Horváth, and C. Córdoba and the availability of data from http://www.msss.com, MOLA, and the Mars Climate Model. The authors also thank Juan Pérez Mercader for the continuous support. S.C.M. acknowledges a Ramón y Cajal contract from the Ministerio de Educación y Ciencia, Spain. Research at the Centro de Astrobiología is supported by the Instituto Nacional de Técnica Aerospacial.

ABBREVIATIONS

GCM, General Circulation Model; MGS, Mars Global Surveyor; MOC, Mars Orbital Camera; MOLA, Mars Orbiter Laser Altimeter; THEMIS, Thermal Emission Imaging System.

REFERENCES

Alton Wade, F. and Negus De Wys, J. (1968) Permafrost features on the martian surface. *Icarus* 9, 175–185.

Arvidson, R.E., Poulet, F., Bibring, J.-P., Wolff, M., Gendrin, A., Morris R.V., Freeman J.J., Langevin, Y., Mangold, N., and Bellucci, G. (2005) Spectral reflectance and morphologic correlations in Eastern Terra Meridiani, Mars. *Science* 307, 1591–1594.

Banin, A., Clark, B.C., and Wänke, H. (1992) Surface chemistry and mineralogy. In *Mars*, edited by H.H. Kieffer, B.M. Jakosky, C.W. Snyder, and M.S. Matthews, University of Arizona Press, Tucson, pp. 594–625.

Bennett, M.R. and Glasser, N.F. (2003) *Glacial Geology—Ice Sheets and Landforms*, John Wiley and Sons, Chichester, UK.

Bibring, J.-P., Langevin, Y., Poulet, F., Gendrin, A., Gondet, B., Berthe, M., Soufflot, A., Drossart, P., Combes, M., Bellucci, Moroz, V., Mangold, N., Schmitt, B., and the OMEGA Team (2004) Perennial water ice identified in the south polar cap of Mars. *Nature* 428, 627–630.

Borisenko, A.S. (1977) Study of the salt composition of solutions in gas-liquid inclusions in minerals by the cryometric method. *Soviet Geol. Geophys.* 18, 11–19.

Boynton, W.V., Feldman, W.C., Squyres, S.W., Prettyman, T.H., Bruckner, J., Evans, L.G., Reedy, R.C., Starr, R., Arnold, J.R., Drake, D.M., Englert, P.A.J., Metzger, A.E., Mitrofanov, I., Trombka, J.I., d'Uston, C., Wanke, H., Gasnault, O., Hamara, D.K., Janes, D.M., Marcialis, R.L., Maurice, S., Mikheeva, I., Taylor, G.J., Tokar, R., and Shinohara, C. (2002) Distribution of hydrogen in the near surface of Mars: evidence for subsurface ice deposits. *Science* 297, 81–85.

Byrne, S. and Ingersoll, A.P. (2003) A sublimation model for martian south polar ice features. *Science* 299, 1051–1053.

Brass, G.W. (1980) Stability of brines on Mars. *Icarus* 42, 20–28.

Cabrol, N.A., Wynn-Williams, D.D., Crawford, D.A., and Grin, E.A. (2001) Recent aqueous environments in impact crater lakes on Mars 2001: an astrobiological perspective. 2nd Mars Polar Conference Special Issue. *Icarus* 154, 98–112.

Christensen, P.R., Wyatt, M.B., Glotch, T.D., Rogers, A.D., Anwar, S., Arvidson, R.E., Bandfield, J.L., Blaney, D.L., Budney, C., Calvin, W.M., Fallacaro, A., Fergason, R.L., Gorelick, N., Graff, T.G., Hamilton, V.E., Hayes, A.G., Johnson, J.R., Knudson, A.T., McSween, H.Y. Jr., Mehall, G.L., Mehall, L.K., Moersch, J.E., Morris, R.V., Smith, M.D., Squyres, S.W., Ruff, S.W., and Wolff, M.J. (2004) Mineralogy at Meridiani Planum from the Mini-TES Experiment on the Opportunity Rover. *Science* 306, 1733–1739.

Clark, B.C. and van Hart, D.C. (1981) The salts of Mars. *Icarus* 45, 370–378.

Córdoba-Jabonero, C., Lara, L.M., Mancho, A.M., Márquez, A., and Rodrígo, R. (2003) Solar ultraviolet transfer in the Martian atmosphere: biological and geological implications. *Planet. Space Sci.* 51, 399–410.

Costard, F., Forget, F., Mangold, N., and Peulvast, J.P. (2002) Formation of recent Martian debris flows by melting of near-surface ground ice at high obliquity. *Science* 295, 110–113.

Fairén, A.G., Fernández-Remolar, D., Dohm, J.M., Baker, V.R., and Amils, R. (2004) Inhibition of carbonate synthesis in acidic oceans on early Mars. *Nature* 431, 423–426.

Feldman, W.C., Boynton, W.V., Tokar, R.L., Prettyman, T.H., Gasnault, O., Squyres, S.W., Elphic, R.C., Lawrence, D.J., Lawson, S.L., Maurice, S., McKinney, G.W., Moore, K.R., and Reedy, R.C. (2002) Global distribution of neutrons from Mars: results from Mars Odyssey. *Science* 297, 75–78.

Fournier, R.O., Thompson, J.M., Cunningham, C.G., and Hutchinson, R.A. (1991) Conditions leading to a recent small hydrothermal explosion at Yellowstone National Park. *GSA Bull.* 103, 1114–1120.

Gaidos, E.J. (2001) Cryovolcanism and the recent flow of liquid water on Mars. *Icarus* 153, 218–223.

Gánti, T., Horváth, A., Bérczy, S., Gesztesi, A., and Szathmáry, E. (2003) Dark dune spots: possible biomarkers on Mars? In *Origins Life and Evolution of the Biosphere, Vol. 33*, Kluwer Academic Publishers, Dordrecht, The Netherlands, pp. 515–557.

Gendrin, A., Mangold, N., Bibring, J.-P., Langevin, Y., Gondet, B., Poulet, F., Bonello, G., Quantin, C., Mustard, J., Arvidson, R., and LeMouelic, S. (2005) Sulfates in Martian layered terrains: the OMEGA/Mars Express View. *Science* 307, 1587–1591.

Gilmore, M.S. and Phillips, E.L. (2002) Role of aquicludes in formation of Martian gullies. *Geology* 30, 1107–1110.

Haberle, M.H., McKay, C.P., Schaeffer, J., Cabrol, N.A., Grin, E.A., Zent, A.P., and Quinn, R. (2001) On the possibility of liquid water on present-day Mars. *J. Geophys. Res.* 106, 23317–23326.

Hartmann, W.K. (2001) Martian seeps and their relation to youthful geothermal activity. *Space Sci. Rev.* 96, 405–410.

Hartmann, W.K., Thorsteinsson, T., and Sigurdsson, F. (2003) Martian hillside gullies and Icelandic analogs. *Icarus* 162, 259–277.

Head, J.W., Mustard, J.F., Kreslavsky, M.A., Milliken, R.E., and Marchant, D.R. (2003) Recent ice ages on Mars. *Nature* 426, 797–802.

Heldmann, J.L. and Mellon, M.T. (2004) Observation of martian gullies and constraints on potential formation mechanisms. *Icarus* 168, 285–304.

Jakosky, B.M., Nealson, K.H., Bakermans, C., Ley, R.E., and Mellon, M.T. (2003) Subfreezing activity of microorganisms and the potential habitability of Mars' polar regions. *Astrobiology* 3, 343–350.

Kargel, J.S. and Lunine, J.I. (1998) Clathrate hydrates on earth and in the solar system. In *Solar System Ices*, edited by B. Schmitt, C. De Bergh, and M. Festou, Kluwer Academic Publishers, Dordrecht, The Netherlands, pp. 97–117.

Kargel, J.S. and Strom, R.G. (1992) Ancient glaciation on Mars. *Geology* 20, 3–7.

Kaufmann, E., Kömle, N.I., and Kargl, G. (2002) Experimental and theoretical investigation of the solid state greenhouse effect. In *ESA Special Publication SP-518: Proceedings of the Second European Workshop on Exo-Astrobiology*, edited by H. Lacoste, ESA Publications Division, Noordwijk, The Netherlands, pp. 87–90.

Kerr, R.A. (2004) Mars—Opportunity tells a salty tale. *Science* 303, 1957.

Kieffer, H.H., Titus, T.N., Mullins, K.F., and Christensen, P.R. (2000) Mars south polar spring and summer behavior observed by TES: seasonal cap evolution controlled by frost grain size. *J. Geophys. Res.* 105, 9653–9699.

Knauth, L.P. and Burt, D.M. (2002) Eutectic brines on Mars: origin and possible relation to young seepage features. *Icarus* 158, 267–271.

Kuznetz, L.H. and Gan, D.C. (2002) On the existence and stability of liquid water on the surface of Mars today. *Astrobiology* 2, 183–195.

Langevin, Y., Poulet, F., Bibring, J.-P., and Gondet, B. (2005) Sulfates in the north polar region of Mars detected by OMEGA/Mars Express. *Science* 307, 1584–1586.

Lewis, S.R., Collins, M., Read, P.L., Forget, F., Hourdin, F., Fournier, R., Hourdin, C., Talagrand, O., and Huot, J.-P. (1999) A climate database for Mars. *J. Geophys. Res.* 104, 24177–24194.

Malin, M.C. and Edgett, K.S. (2001) Mars Global Surveyor Mars Orbiter Camera: interplanetary cruise through primary mission. *J. Geophys. Res.* 106, 23429–23570.

Malin, M.C., Caplinger, M.A., and Davis, S.D. (2001) Observational evidence for an active surface reservoir of solid carbon dioxide on Mars. *Science* 294, 2146–2148.

Mangold, N., Maurice, S., Feldman, W.C., Costard, F., and Forget, F. (2004) Spatial relationships between patterned ground and ground ice detected by the Neutron Spectrometer on Mars. *J. Geophys. Res.* 109, E08001.

Marion, G.M. (2002) Modeling aqueous ferrous iron chemistry at low temperatures with application to Mars. *Geochim. Cosmochim. Acta* 67, 4251–4266.

Marion, G.M., Catling, D.C., and Kargel, J.S. (2003) Modeling aqueous ferrous iron chemistry at low temperatures with application to Mars. *Geochim. Cosmochim. Acta* 67, 4251–4236.

Mellon, M.T. and Phillips, R.J. (2001) Recent gullies on Mars and the source of liquid water. *J. Geophys. Res.* 106, 23165–23179.

Mitrofanov, I., Anfimov, D., Kozyrev, A., Litvak, M., Sanin, A., Tret'yakov, V., Krylov, A., Shvetsov, V., Boynton, W., Shinohara, C., Hamara, D., and Saunders, R.S. (2002) Maps of subsurface hydrogen from the high energy neutron detector, Mars Odyssey. *Science* 297, 78–81.

Morris, R.V., Ming, D.W., Clark, B.C., Klingelhoefer, G., Gellert, R., Rodionov, D., Schroeder, C., de Souza, P.A., Yen, A., and the Athena Science Team (2005) Abundance and speciation of water and sulfate at Gusev Crater and Meridiani Planum [abstract 2239]. In *36th Lunar and Planetary Science Conference Abstracts*, LPI Contribution No. 1234, Lunar and Planetary Institute, Houston.

Musselwhite, D.S., Swindle, T.D., and Lunine, J.I. (2001) Liquid CO_2 breakout and the formation of recent small gullies on Mars. *Geophys. Res. Lett.* 28, 1283–1285.

Piqueux, S., Byrne, S., and Richardson, M.I. (2003) Sublimation of Mars's southern seasonal CO_2 ice cap and the formation of spiders. *J. Geophys. Res.* 108, 5084.

Prieto-Ballesteros, O. and Kargel, J.S. (2005) Thermal state and complex geology of a heterogeneous salty crust of Jupiter's satellite, Europa. *Icarus* 173, 212–221.

Rieder, R., Economou, T., WÑnke, H., Turkevich, A., Crisp, J., BrÅckner, J., Dreibus, G., and McSween, H.Y. Jr. (1997) The chemical composition of Martian soil and rocks returned by the mobile Alpha Proton X-ray Spectrometer: preliminary results from the x-ray mode. *Science* 278, 1771–1774.

Smith, M.D., Bandfield, J.L., Christensen, P.R., and Richardson, M.I. (2003) Thermal Emission Imaging System (THEMIS) infrared observations of atmospheric dust and water ice cloud optical depth. *J. Geophys. Res.* 108, doi: 10.1029/2003JE002115.

Tanaka, K.L. and Kolb, E.J. (2001) Geologic history of the polar regions of Mars based on Mars Global Surveyor data. I. Noachian and Hesperian Periods. *Icarus* 154, 3–21.

Titus, T.N., Kieffer, H.H., and Christensen, P.R. (2003) Exposed water ice discovered near the south pole of Mars. *Science* 299, 1048–1051.

Treiman, A.H. (2003) Geologic settings of Martian gullies: implications for their origins. *J. Geophys. Res.* 108, doi: 10.1029/2002JE001900.

Wynn-Williams, D.D., Cabrol, N.A., Grin, E.A., Haberle, R.M., and Stoker, C.R. (2001) Brines in seepage channels as eluents for subsurface relict biomolecules on Mars? *Astrobiology* 2, 165–184.

Address reprint requests to:
Olga Prieto-Ballesteros
Centro de Astrobiología
Instituto Nacional de Técnica Aeroespacial-Consejo Superior de Investigaciones Científicas
Ctra. Ajalvir km. 4
28850 Torrejón de Ardoz
Madrid, Spain

E-mail: prietobo@inta.es